Hindawi Publishing Corporation
International Journal of Antennas and Propagation
Volume 2011, Article ID 438437, 12 pages
doi:10.1155/2011/438437

*Research Article*

# A Modal Description of Multiport Antennas

**Jonathan J. Lynch**

*Microelectronics Laboratory, HRL Laboratories, LLC, Malibu, CA 90265, USA*

Correspondence should be addressed to Jonathan J. Lynch, jjlynch@hrl.com

Received 15 February 2011; Revised 27 April 2011; Accepted 15 June 2011

Academic Editor: Miguel Ferrando



This paper presents a modal description of multiport antennas that leads directly to a rigorous network representation and simple quadratic expressions for gain, efficiency, and effective area. The analysis shows that the transmitting and receiving properties of an $N$ element antenna array are exactly described by a $2N \times 2N$ element scattering matrix together with a set of $N$ orthonormal mode functions and accounts for effects such as mutual coupling, scattering, reflection, and losses. The approach is quite general, only requiring that the antenna be finite and reciprocal. The scattering network description simplifies accounting of power flow while retaining a close connection to the physical antenna characteristics. The orthonormal mode functions provide a complete basis for radiated and received fields, facilitating beamforming. The theory provides rigorous definitions of input-output signals and links them to the underlying electromagnetics in a straightforward manner.

## 1. Introduction

Many communications, radar, and sensing systems rely on arrays of antenna elements, each with individual receivers, to transmit or receive energy with radiation patterns that may be manipulated in real time by digitally modifying the coherent combination of received signals. The flexibility afforded by such digital beamforming allows, for example, a radar system to electronically track multiple targets with the sensitivity afforded by high gain beams, a high data rate receiving system to communicate simultaneously with multiple users on channels with high spatial selectivity, or a direction finding system capable of locating many emitters with high accuracy. Multiple input, multiple output (MIMO) communication systems in particular have demonstrated robust data transfer in the presence of multipath interference as a result of the redundancy provided by multiple independent spatial channels [1].

The development of the underlying signal processing of such systems typically begins with abstract and often idealized constructs where the signals transmitted and received by individual antenna elements are represented as time-(or phase-) shifted replicas that depend in a straightforward way on the antenna geometry. Often neglected from such analyses are the effects of mutual scattering and coupling between elements as well as scattering from objects in the vicinity of the antenna. A perturbation approach is often utilized in system design to provide first order corrections due to such coupling and scattering with mixed and sometimes contradictory results reported in the literature [2]. A scattering description of MIMO systems has been presented in [3, 4] that takes into account coupling between antenna elements. However, this analysis defines the scattering parameters with respect to a fixed location in the far field and must be modified for different incident/radiation angles. This approach does include structural scattering, although this is generally not important for MIMO arrays.

The analytical description of a multiport antenna has typically been provided by the terminal port impedance, admittance, or scattering matrix together with radiation patterns obtained by successively exciting each port with the others terminated in known loads. Linear combinations of the resulting field patterns are used to obtain desired beam shapes. For the receiving case, equivalent circuits have been developed that allow calculation of the received signals for a multiport antenna under plane wave incidence, including mutual coupling and scattering. For example, [5] provides a rigorous derivation of such an equivalent circuit in the frequency domain and [6] provides the same in the time domain. Alternatively, [7] describes an $N$ element multiport antenna by including a test antenna and considering the resulting $N + 1$ element antenna system. This approach leads

to expressions for antenna gain in terms of the mutual impedance (or admittance) between the multiport and test antennas.

This paper presents a modal approach to multiport antennas that provides an exact description of the transmitting and receiving properties of the antenna and leads to quadratic expressions for antenna parameters of interest, such as gain, efficiency, and effective area. The theory shows that a finite multiport antenna with $N$ pairs of feed terminals (i.e., ports) will produce exactly $N$ orthogonal "radiation" modes whose linear combinations may describe any possible transmit or receive pattern for that array (assuming the terminal port excitations produce linearly independent far zone fields, as is nearly always the case in practice). The scattering network description together with the mode functions completely characterize the transmitting and receiving properties of an antenna, although these modes are not sufficient to completely describe scattering by the antenna due to incident waves.

The analysis presented here is quite general and applies to a large class of antennas. The fundamental assumptions are that the antenna is comprised of linear materials and is finite so that far fields may be asymptotically defined in empty space at a suitably large distance. Because the antenna is assumed finite, this analysis does not apply to (for example) infinite periodic structures, although one could represent each of the Floquet modes as a radiation port applying the same techniques. We also assume the antenna elements and nearby materials are reciprocal to facilitate the analysis of the receive case, although this assumption is not necessary to define the radiation modes. Unlike other antenna modal analyses, this theory allows for dissipation within and around the antenna.

A different but related modal description was developed in the 1960s by Garbacz and Turpin [8] and Harrington and Mautz [9] first for scattering bodies and later for antenna arrays [10]. Their approach was to determine a set of orthogonal excitations that effectively eliminate mutual coupling between elements. We distinguish these as "backscatter" modes. In the lossless case, the radiation and backscatter modes are identical, a fact that limited the previous modal analyses to the lossless case [11]. For antennas with finite conductivity and dielectric losses, the backscatter modes do not produce orthogonal radiated fields and therefore may not be as useful for beamforming as the radiation modes. Backscatter modes and their associated decoupling networks are useful for other purposes and various groups have explored their application [12]. We include a short discussion of backscatter modes in this paper to place them in context with radiation modes and show how both mode sets diagonalize different portions of the complete $2N \times 2N$ antenna scattering matrix.

Following the Introduction (Section 1), this paper is organized into five additional sections. In Section 2, we show how to derive the radiation mode set from antenna measurements. These modes provide a complete orthonormal basis for all possible fields radiated from and received by the antenna. We again note that our modal description is not sufficient to describe the so-called structural mode scattering by the antenna resulting from external energy sources. Problems such as low RCS antenna design require a fuller basis, such as spherical harmonics, to support general antenna scattering. In Section 3, the radiation modes are used to define an antenna scattering matrix, providing a complete network description of the antenna. In addition to the usual terminal port scattering parameters, this matrix also includes parameters describing transmission, reception, and antenna-mode (as opposed to structural mode) scattering. Here, we show that an ideal transformation network that produces the radiation mode excitations diagonalizes the scattering submatrices for transmission ($S_{21}$), and reception ($S_{12}$), and show the close connection between $S_{21}$ and antenna efficiency. In Section 4, we apply the formalism to produce simple quadratic expressions for antenna efficiency, directivity, and gain and derive the relation between gain and effective area for an arbitrary multiport antenna. In Section 5, we define the backscatter modes as the solutions to a conjugate eigenvalue problem and show how a transformation (i.e., decoupling) network diagonalizes the reflection coefficient submatrix $S_{11}$. These two different diagonalizations distinguish the modes sets: one leads to orthonormal-radiated fields and an equivalent network description, the other to decoupled terminal ports. Finally, in Section 6, we present two examples illustrating the application of the theory.

## 2. Radiation Modes

A multiport antenna consisting of $N$ elements, each with a pair of feed terminals (or a waveguide port), is capable of transmitting or receiving a variety of field patterns. The so-called element patterns of the antenna are produced by exciting each of the feed terminals separately with the ports terminated in known impedances. The element patterns are similar to translated versions of the pattern produced by exciting a single element in isolation but are altered by the coupling between, and scattering by, neighboring elements. Because the materials comprising the antenna are assumed linear, superposition holds and the $N$ complex incident wave amplitudes provide $N$ (complex) degrees of freedom that span the space of all possible radiated fields from the array. For a reciprocal antenna, the transmitting and receiving element patterns are identical so the receiving antenna possesses the same $N$ (complex) degrees of freedom. It is important to note that we distinguish "radiated" field patterns, which are due to terminal port excitations, from "scattered" field patterns, which may result (for example) from plane wave incidence. The space of complex fields spanned by all linear combinations of incident terminal port wave amplitudes represents radiated fields but is not sufficient to describe the scattered fields. The portion of scattered fields that lies in this space is called "antenna mode" scattering, and the portion outside this space is called "structural mode" scattering.

To facilitate power flow computations, we define a $2N \times 2N$ scattering matrix that represents an $N$ element multiport antenna. Such a network description of antennas was first

proposed in [13], with more detail provided in [14], which utilized spherical modes to define the far field "ports". Because the infinite set of spherical modes is sufficient to describe arbitrary field distributions, this approach describes not only the transmitting and receiving properties of the antenna, but also the structural scattering due to incident fields. When knowledge of these structural scattering properties is not needed, as is often the case in practice, one may reduce the set to exactly $N$ modes (generally equal to the number of terminal ports) that provide a complete basis for radiated and received fields.

First, some remarks must be made concerning antenna ports. At the terminal side of the array, we use the definitions of ports and associated voltages, currents, and incident/reflected waves from microwave circuit theory. Rigorous definitions of equivalent terminal ports have been presented in detail elsewhere (e.g., see [15–17]) and need not be repeated here. On the radiation side of the array, we must begin by defining equivalent circuit "radiation" ports and we do this by requiring that the power flowing to and from each port be independent of power flowing in the other ports. This condition is implicitly assumed in any set of circuit ports and will be met if and only if the set of port fields is orthogonal. We note that on the terminal side of the array this is often satisfied through isolation. For example, coaxial cables have (assumed) perfect field confinement. If a physical connection supports multiple modes (e.g., overmoded waveguide), each of the (orthogonal) modes may be represented by a separate port in the equivalent network. On the radiation side of the array, we must determine an orthogonal set of fields that supports all possible radiated patterns in order to properly define equivalent radiation ports.

*2.1. Transmitting.* Consider waves incident upon the antenna input terminals and radiated by the antenna elements (i.e., the transmitting case). Exciting the $n$th terminal port with one Watt of time average incident power at zero phase with all other ports terminated in their reference impedances produces a far zone electric field $\overline{E}_n(r,\theta,\phi)$ (we use RMS field amplitudes throughout this paper), described with respect to a spherical coordinate system with the origin of some fixed location within or near the antenna. We seek linear combinations of these outward traveling waves

$$\overline{E}_n^- = \sum_{m=0}^{N-1} U_{m,n}\overline{E}_m \tag{1}$$

that form an orthogonal set in the far field:

$$\begin{aligned}\frac{1}{\eta_o}\iint \overline{E}_p^{-*}\cdot\overline{E}_q^- dS &= \sum_m\sum_n U_{m,p}^*\left[\frac{1}{\eta_o}\iint \overline{E}^*{}_m\cdot\overline{E}_n dS\right]U_{n,q}\\ &= \sum_m\sum_n U_{m,p}^* M_{m,n}U_{n,q} = \left|\lambda_p\right|^2\delta_{p,q},\end{aligned} \tag{2}$$

where $\eta_o = \sqrt{\mu_o/\varepsilon_o}$ is the intrinsic impedance of free space, $\delta$ is the Kronicker delta function, and the asterisk denotes complex conjugate. The negative superscript indicates outgoing waves, and a positive superscript will indicate incoming waves. The differential area is $dS = r^2\sin\theta d\theta\, d\phi = r^2 d\Omega$, and the integration extends over the entire sphere $0 < \theta < \pi$, $0 < \phi < 2\pi$ as $r \to \infty$.

Each element of the matrix

$$M_{m,n} = \frac{1}{\eta_o}\iint \overline{E}^*{}_m\cdot\overline{E}_n dS \tag{3}$$

is proportional to the overlap integral of the fields produced by two terminal-port excitations. Expressing last equality of (2) in matrix notation, we have

$$U^H M U = \Lambda^H\Lambda, \tag{4}$$

where the superscript indicates the Hermitian conjugate transpose. The orthogonal fields $\overline{E}_n^-$ and $\overline{H}_n^- = (1/\eta_o)\hat{u}_r\times\overline{E}_n^-$ will be referred to as radiation mode fields, with each mode representing a radiation port in a manner similar to port definitions of uniform waveguides [17]. The diagonal matrix $\Lambda$ contains complex parameters $\lambda_n$, whose magnitude squared turns out to be the total efficiency for the $n$th mode. The coefficient matrix $U$ contains the eigenvectors of $M$ as its columns, each column providing the incident wave amplitudes for the corresponding mode excitation. We note that the eigenvector matrix $U$ is not unique since each column may be multiplied by a phase factor while still satisfying (4). Once the matrix $U$ is specified, one may compute the modal fields from the terminal port excited radiation fields using (1).

Because $M$ is Hermitian, we are guaranteed a set of $N$ orthogonal modes, one for each set of terminal pairs, for nearly all practical cases of interest (we ignore pathological cases where two terminal ports produce linearly dependent radiated fields). We assume for simplicity that the number of radiating elements is equal to the number of terminal ports, but this is not necessary. The theory applies equally well when there are fewer terminal ports than radiating elements. For this case, the number of radiation modes is equal to the number of terminal ports, not the number of antenna elements.

In the far field of the antenna, the radiation mode fields are spherical waves proportional to equivalent circuit voltage amplitudes:

$$\overline{E}_n^-(r,\theta,\phi) = V_n^-\frac{e^{-jkr}}{r}\hat{e}_n(\theta,\phi), \tag{5}$$

where $V_n^-$ is the outward traveling (complex constant) voltage amplitude and $k = \omega\sqrt{\mu_o\varepsilon_o}$. The complex vector mode functions $\hat{e}_n = \hat{u}_n e_n$ (with unit polarization vector $\hat{u}_n$) are scaled to form an orthonormal set:

$$\iint \hat{e}_n\cdot\hat{e}_m^*\, d\Omega = \delta_{n,m}. \tag{6}$$

The field representation (5) with orthonormal mode functions is the same as that used for uniform waveguides. We note that (6) allows the phase of each mode function $\hat{e}_n$ to be arbitrarily chosen. Inserting (5) into (2) and using (6), we

find that $|V_n^-|^2 = \eta_o|\lambda_n|^2$, so that the radiation mode fields are related to the normalized mode functions as

$$\overline{E}_n^-(r,\theta,\phi) = \sqrt{\eta_o}\lambda_n\hat{e}_n(\theta,\phi)\frac{e^{-jkr}}{r}. \quad (7)$$

Equating (7) with (1), we may determine the complex $\lambda_n$ directly from the measured fields:

$$\lambda_n = \frac{1}{\sqrt{\eta_o}}e^{jkr}\sum_m U_{mn}\iint r\overline{E}_m\cdot\hat{e}_n^*\,d\Omega. \quad (8)$$

Generally, spherical waves from an arbitrary source can be expanded in terms of spherical modes that are products of spherical Bessel functions and Tesseral harmonics, with associated mode propagation constants and mode impedances. In the far field, the radial dependences of all the modes asymptotically approach the form (5), the propagation constants approach the value $k$, and the wave impedances approach $\eta_o$. Thus, the far field spherical modes are degenerate so that any linear combination is also a mode. The relation between the modal fields and voltages given in (5) is therefore consistent with (but different from) the microwave circuit formalism of [16]. Our modal representation takes advantage of the high degree of degeneracy to represent the fields in a manner convenient for antenna engineering and measurement.

As a result, we may describe the radiated mode fields in terms of an equivalent circuit, as indicated in Figure 1. Each of the modal field amplitudes is represented by a traveling wave voltage on a radial transmission line of characteristic impedance $\eta_o$, one for each mode. The orthogonality of the modal fields ensures that the total radiated power is the sum of the powers traveling on each radial line.

An arbitrary field $\overline{E}$ radiated from the antenna may be expressed as a superposition of mode functions

$$\overline{E} = \sum_{n=0}^{N-1} V_n^-\frac{e^{-jkr}}{r}\hat{e}_n(\theta,\phi), \quad (9)$$

and we may determine the equivalent voltage amplitudes using orthogonality (6):

$$V_n^-\frac{e^{-jkr}}{r} = \iint\overline{E}(r,\theta,\phi)\cdot\hat{e}_n^*(\theta,\phi)\,d\Omega. \quad (10)$$

The directive gain pattern $D_n$ for the $n$th radiation port is related to the mode functions using (5) and (6):

$$D_n(\theta,\phi) = \frac{4\pi\left|\overline{E}_n^-\right|^2}{\iint\left|\overline{E}_n^-\right|^2 d\Omega} = 4\pi\left|\hat{e}_n\right|^2. \quad (11)$$

The gain in the $\theta,\phi$ direction for an arbitrary radiated field (9) may be computed using (6):

$$D(\theta,\phi) = \frac{4\pi\left|\overline{E}(\theta,\phi)\right|^2}{\iint\left|\overline{E}(\theta,\phi)\right|^2 d\Omega} = 4\pi\frac{V^{-H}[\hat{e}^*\cdot\hat{e}^T]V^-}{V^{-H}V^-}, \quad (12)$$

where $V^-$ (without subscript) is an $N$ element vector representing the voltages of the outgoing waves, and the matrix $[\hat{e}^*\cdot\hat{e}^T]_{m,n} \equiv \hat{e}_m^*\cdot\hat{e}_n$ expresses the outer product. We will find this matrix notation convenient in later sections.

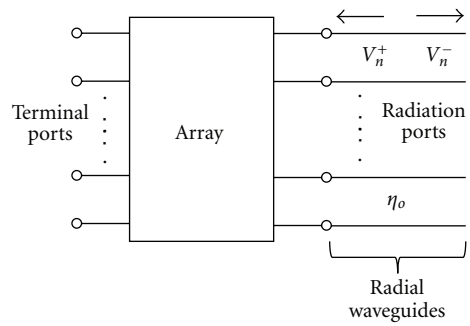


Figure 1: Radiated fields are represented by radial waveguides, one per mode, whose amplitudes are given by the traveling wave voltages and currents. Orthogonality of the modal fields ensures that power flows independently along the radial guides.

*2.2. Receiving.* The receiving properties of the antenna may be determined by application of Lorentz's reciprocity relation, as was done in [15]. We take a different approach, noting that the time reversal properties of Maxwell's equations in free space suggest that the antenna receives energy in modes that are the conjugate of the transmission mode functions,

$$\overline{E}_n^+(r,\theta,\phi) = V_n^+\frac{e^{jkr}}{r}\hat{e}_n^*(\theta,\phi). \quad (13)$$

One may verify that the conjugate ensures the correct polarization matching as well as collocated phase centers for transmit and receive. Because the transmitting and receiving mode functions are different, the circuit formalism is not the same as for standard circuits. Incoming and outgoing waves travel on equivalent transmission lines with different mode functions, although we represent them together pictorially (see Figure 1) for convenience. When the mode functions are real, the standard waveguide network formalism applies, and this occurs when the coordinate system is located at the phase center of the mode. Allowing the incoming and outgoing mode functions to be different departs from conventional circuit theory, but this eliminates the need to determine modal phase centers, something that is difficult to accomplish in practice.

We may use the receiving mode functions to compute the available power for a plane wave incident from the $\theta_o,\phi_o$ direction. Assuming an $E$ field polarization unit vector $\hat{u}_{\text{pw}}$ and amplitude $E_o$, the incident field is

$$\overline{E}_{\text{pw}} = \hat{u}_{\text{pw}}E_o e^{j\overline{k}\cdot\overline{r}} = \hat{u}_{\text{pw}}E_o e^{jkr[\sin\theta_o\sin\theta\cos(\phi-\phi_o)+\cos\theta_o\cos\theta]}. \quad (14)$$

We represent this plane wave as a linear combination of incoming receive modes:

$$\overline{E}_{\text{pw}} \approx \sum_{m=0}^{N-1} V_m^+\frac{e^{jkr}}{r}\hat{e}_m^*(\theta,\phi). \quad (15)$$

Note that the superposition (15) is only an approximation to the incident plane wave field since the mode functions are not a sufficient basis for arbitrary field distributions.

Structural scattering is scattered field energy not supported by the mode function basis.

The incident voltage amplitudes are determined from (15) using orthogonality,

$$V_n^+ \frac{e^{jkr}}{r} = \iint \overline{E}_{\text{pw}} \cdot \hat{e}_n(\theta,\phi)\, d\Omega = E_o \iint \hat{u}_{\text{pw}} \cdot \hat{e}_n \times e^{jkr[\sin\theta_o \sin\theta\cos(\phi-\phi_o)+\cos\theta_o\cos\theta]} d\Omega. \tag{16}$$

This integral may be evaluated asymptotically as $r \to \infty$ using the method of steepest descents, with details given in the appendix A. We find the equivalent voltage amplitude for the incident wave is

$$V_n^+ = -j\lambda E_o \hat{u}_{\text{pw}} \cdot \hat{e}_n(\theta_o,\phi_o) = -j\lambda \overline{E}_{\text{pw}} \cdot \hat{e}_n, \tag{17}$$

where $\lambda$ is the wavelength of the incident radiation. This expression relates the equivalent voltage to the amplitude, direction, and polarization of the incident plane wave. The network model for plane wave incidence is shown in Figure 2. The expressions for the equivalent voltage sources in Figure 2 are similar to those derived in [5]. One must keep in mind that each radiation port in Figure 2 represents a single mode and is comprised of contributions from all of the antenna elements.

The time average incident power at the $n$th radiation port may be expressed in terms of the radiation pattern using (17) with (11):

$$P_{\text{inc},n} = \frac{\left|V_n^+\right|^2}{\eta_o} = \frac{|E_o|^2}{\eta_o}\lambda^2 \left|\hat{u}_{\text{pw}} \cdot \hat{u}_n\right|^2 |e_n|^2 = S_{\text{pw}} \frac{\lambda^2}{4\pi} D_n \left|\hat{u}_{\text{pw}} \cdot \hat{u}_n\right|^2, \tag{18}$$

where $S_{\text{pw}}$ is the average power density in the incident plane wave and the last factor accounts for polarization mismatch. We note that the polarization mismatch factor $|\hat{u}_{\text{pw}} \cdot \hat{u}_n|^2$ differs from that given in [18] by a complex conjugate. This is due to differences in our definitions of the plane wave polarization vector.

Equation (18) confirms the well-known expression for available receive power in terms of the maximum effective area of the antenna and shows how it arises from an overlap integral of the plane wave with the mode function. The maximum power available to the antenna is the sum of the incident powers from all the modes,

$$P_{\text{avail}} = \sum_n P_{\text{inc},n} = S_{\text{pw}} \frac{\lambda^2}{4\pi} \sum_n D_n \left|\hat{u}_{\text{pw}} \cdot \hat{u}_n\right|^2, \tag{19}$$

showing that the maximum available directive gain is the sum of the radiation mode gains. The power collected by the terminal ports depends on the scattering parameters of the antenna array and will be considered in the next section.

We now have a network description of the incident and radiated fields for an $N$ element multiport antenna in terms of equivalent voltages and currents on radial transmission lines that represent the network port terminations and have related the voltages and currents to the radiating/received fields through a set of $N$ normalized field functions. In the next section, we relate the incident, reflected, radiated, and received fields through a scattering matrix.

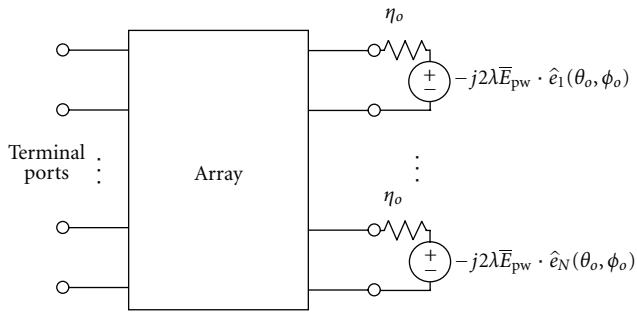


Figure 2: For the receiving case, an incident plane wave may be represented by a set of equivalent voltage sources, one for each mode.

## 3. Scattering Matrix Representation

Incident and scattered waves may be defined in the usual way with respect to the (RMS) traveling wave voltages: $a_n = V_n^+/\sqrt{\eta_o}$ and $b_n = V_n^-/\sqrt{\eta_o}$, where the port voltage is $V_n = V_n^+ + V_n^-$ and the current entering the port is $I_n = I_n^+ - I_n^-$. The scattering matrix describes the interactions within the antenna between the incoming and outgoing waves using $b = Sa$:

$$\begin{pmatrix} b_1 \\ b_2 \end{pmatrix} = \begin{pmatrix} S_{11} & S_{12} \\ S_{21} & S_{22} \end{pmatrix} \begin{pmatrix} a_1 \\ a_2 \end{pmatrix}, \tag{20}$$

where $S_{11}$, and so forth, are $N \times N$ submatrices and $a_1$, and so forth, are $N$ element vectors. The subscript "1" denotes the terminal side of the array, and the subscript "2" denotes the radiation side. Thus, $S_{11}$ is the scattering matrix at the array terminal ports that is typically measured with a vector network analyzer. $S_{21}$ describes the transmitted waves for terminal port excitation, $S_{12}$ describes received waves at the terminal ports due to incident fields, and $S_{22}$ describes waves scattered into the outgoing port fields due to incident fields. As mentioned above, the far field scattering properties of a multiport antenna are not completely described by $S_{22}$. In general, a portion of the total scattered energy will be orthogonal to all of the port fields. Our analysis does not represent such structural mode scattering.

The radiation submatrix $S_{21}$ may be determined from antenna measurements in the following way. One applies a continuous wave signal (scaled to unity power and zero phase) to each of the elements in turn with the other elements terminated in their respective port reference impedances and measures the radiated far zone complex vector electric fields $\overline{E}_n(r,\theta,\phi)$. The port field functions are computed using (1)–(6) and the amplitudes using (10) (with $V_n^+ = 0$ at the radiation ports). The $n$th radiated port wave at

radial distance $r$ due to "unit" excitation of the $m$th antenna terminal is

$$S_{21,nm} = b_{2,n}\big|_{a_{1,m}=1} = \frac{1}{\sqrt{\eta_o}} \iint r\overline{E}_m \cdot \hat{e}_n^* \, d\Omega = U_{mn}^* \lambda_n e^{-jkr}. \tag{21}$$

To arrive at the last expression, we used $U^H U = I$ together with (8), noting $\overline{E}_n = 0$ for $m \neq n$. In (21), the radiation port reference planes are all located at the radial distance $r$, but these may be moved to any desired location by selecting the value of $r$ for each port. It is often convenient to refer the radiation port phases to $r = 0$.

Expressing $S_{21}$ in matrix form (with $r = 0$),

$$S_{21} = \Lambda U^H, \tag{22}$$

where $\Lambda$ is a diagonal matrix whose diagonal elements are $\lambda_n$. Using (22), we may now identify the matrix in (3) as $M = {S_{21}}^H S_{21}$ and the columns of $U$ as the incident wave vectors $a_1$ that produce the corresponding mode fields. Although there are many orthonormal sets of radiated fields for an antenna (any unitary transformation of the mode field functions gives another orthonormal set), our particular choice is the one that results in an orthonormal set of incident terminal port wave vectors.

The matrix $S_{12}$ describes the receiving properties of the antenna. Using (17), we may determine the incident port waves (at reference plane $r = 0$) corresponding to the plane wave in (16):

$$a_{2,n} = -j\lambda \frac{1}{\sqrt{\eta_o}} \overline{E}_{\text{pw}} \cdot \hat{e}_n. \tag{23}$$

In principle, we may determine the scattering parameters $S_{12}$ by measuring the terminal port outputs due to incident plane wave fields. However, for reciprocal antennas, $S_{12} = S_{21}^T$, so these measurements are unnecessary.

The matrix $S_{22}$ describes energy backscattered into the radiation port fields due to incident plane waves (or superpositions of plane waves), often referred to as antenna mode scattering. In principle, one may determine $S_{22}$ by measuring or simulating the scattered fields due to plane waves incident from various directions, but we leave this analysis beyond the scope of this paper. In practice, the backscattered waves are often unimportant. An exception is low RCS antenna design where both the antenna mode and structural mode scattered fields are important.

Using (22), the full antenna scattering matrix may be expressed as

$$S = \begin{pmatrix} S_{11} & U^*\Lambda \\ \Lambda U^H & S_{22} \end{pmatrix}. \tag{24}$$

The sets of incident waves that produce the radiation modes may (in theory) be generated using a lossless, reciprocal transformation network, illustrated in Figure 3, whose scattering matrix is

$$S_U = \begin{pmatrix} 0 & U^T \\ U & 0 \end{pmatrix}. \tag{25}$$

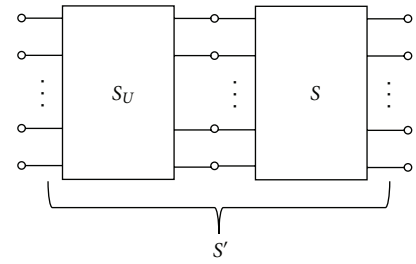


Figure 3: A transformation network placed on the terminal side of the array produces the mode excitations. For example, a wave incident upon a port on the left side of $S_U$ produces the corresponding set of modal incident waves at the antenna terminals. This transformation network diagonalizes the antenna S parameter submatrices $S_{21}$ and $S_{12}$.

The scattering matrix for the combined transformation network and antenna is

$$S' = \begin{pmatrix} U^T S_{11} U & \Lambda \\ \Lambda & S_{22} \end{pmatrix} \tag{26}$$

showing that this mode transformation diagonalizes the radiation and reception submatrices.

To illustrate the formalism, we will compute the waves received by one array (antenna II) due to terminal port incident waves radiated by another (antenna I). This may be useful for MIMO antenna analysis, although here we assume a perfect channel (empty space) for simplicity. The waves received by antenna II are $b_1^{\text{II}} = S_{12}^{\text{II}} a_2^{\text{II}}$. The waves incident upon antenna II may be related to incident electric field due to antenna I $\overline{E}^{\text{I}}$ using (23):

$$a_2^{\text{II}} = -j\lambda \frac{1}{\sqrt{\eta_o}} \overline{E}^{\text{I}} \cdot \hat{e}^{\text{II}}. \tag{27}$$

But this electric field may be expressed in terms of outgoing waves from antenna I using (9):

$$\overline{E}^{\text{I}} = \sum_n \sqrt{\eta_o} b_{2,n}^{\text{I}} \hat{e}_n^{\text{I}} \frac{e^{-jkr}}{r}. \tag{28}$$

Inserting (28) into (27) and using $b_2^{\text{I}} = S_{21}^{\text{I}} a_1^{\text{I}}$, we have

$$b_1^{II} = -j\lambda \frac{e^{-jkr}}{r} S_{12}^{\text{II}} \left[ \hat{e}^{\text{II}} \cdot \left( \hat{e}^{\text{I}} \right)^T \right] S_{21}^{\text{I}} a_1^{\text{I}}, \tag{29}$$

where the mode overlap matrix uses the notation described just below (12), namely $[\hat{e}^{\text{II}} \cdot (\hat{e}^{\text{I}})^T]_{m,n} = \hat{e}_m^{\text{II}} \cdot \hat{e}_n^{\text{I}}$. This result expresses the scattering parameter $S_{21}^{\text{total}}$ between the two sets of antenna terminals in terms of the antenna $S$ parameters and mode functions. Following the same analysis with antenna II transmitting and antenna I receiving produces $S_{12}^{\text{total}} = (S_{21}^{\text{total}})^T$, confirming reciprocity.

We see that the result of cascading antenna scattering networks is different than for microwave circuits. The reason is that each antenna mode set depends on the physical location of that antenna. When two identical antennas are

separated, their mode patterns are different and this is taken into account by a mode overlap matrix, which in our present case is $[\hat{e}^{\mathrm{II}} \cdot (\hat{e}^{\mathrm{I}})^T]$. A realistic communications channel contains multipath scattering from objects such as the ground or buildings that further mixes the modes between the two antennas. However, as long as these scattering events are in the far fields of the antennas, our analysis correctly accounts for mutual coupling and scattering between antenna elements.

## 4. Efficiency, Gain, and Effective Area

The multiport antenna scattering parameters and mode functions allow us to compute various antenna parameters, such as efficiency, gain, and effective area, in a straightforward manner. The total efficiency (including reflection and dissipative losses) for a particular excitation is defined as the ratio of the total radiated power to the incident power

$$\varepsilon_{\mathrm{tot}} = \frac{b_2^H b_2}{a_1^H a_1} = \frac{a_1^H S_{21}^H S_{21} a_1}{a_1^H a_1}. \tag{30}$$

It is useful to define mode efficiencies, the total efficiency when the terminal ports are excited by a mode vector (i.e., $a_1$ is equal to a column of $U$). Using (22), these are given by the diagonal elements of

$$\frac{U^H S_{21}^H S_{21} U}{U^H U} = \Lambda^H \Lambda, \tag{31}$$

which are just the eigenvalues $|\lambda_n|^2$ of $M = S_{21}^H S_{21}$. Thus, we identify $\Lambda^H\Lambda$ as the (diagonal) mode efficiency matrix.

The directive gain may be expressed in terms of the outgoing waves $b_2 = V_2^-/\sqrt{\eta_o}$ using (12) and the incident terminal port waves using $b_2 = S_{21}a_1$:

$$D(\theta,\phi) = 4\pi \frac{a_1^H S_{21}^H [\hat{e}^* \cdot \hat{e}^T] S_{21} a_1}{a_1^H S_{21}^H S_{21} a_1}, \tag{32}$$

showing how the directive gain pattern depends on the excitations $a_1$. The power gain relates the radiated power density to the power accepted by the antenna terminals. In terms of the incident wave vector, the power gain is

$$G_p(\theta,\phi) = 4\pi \frac{a_1^H S_{21}^H [\hat{e}^* \cdot \hat{e}^T] S_{21} a_1}{a_1^H \left(I - S_{11}^H S_{11}\right) a_1}. \tag{33}$$

Finally, the realized gain (that we indicate without subscript) relates the radiated power density to the incident power

$$G(\theta,\phi) = 4\pi \frac{a_1^H S_{21}^H [\hat{e}^* \cdot \hat{e}^T] S_{21} a_1}{a_1^H a_1}. \tag{34}$$

For the receiving case, we may again relate the effective area to the transmitting gain, but we must specify exactly what gain we mean since (32), (33), and (34) supply infinite possibilities, each depending on the choice of incident waves $a_1$. Considering the plane wave given in (14), the incident wave amplitudes $a_2$ may be computed using (17). The result is

$$e_{\mathrm{pw},n}(\theta_o,\phi_o) = \hat{u}_{\mathrm{pw}} \cdot \hat{e}_n(\theta_o,\phi_o), \tag{35}$$

which is the scalar components of the vector field functions in the polarization direction of the incident plane wave, so that $a_{2,n} = -j\lambda(E_o/\sqrt{\eta_o})e_{\mathrm{pw}}$. Using this notation with (22), $b_1 = S_{12}a_2$, and $S_{12} = S_{21}^T$, we find that the total power collected by the antenna terminals is

$$b_1^H b_1 = \lambda^2 \frac{|E_o|^2}{\eta_o} e_{\mathrm{pw}}^H S_{12}^H S_{12} e_{\mathrm{pw}} = \lambda^2 \frac{|E_o|^2}{\eta_o} e_{\mathrm{pw}}^H \Lambda^H \Lambda e_{\mathrm{pw}}, \tag{36}$$

so that the effective area is

$$A_e(\theta_o,\phi_o) = \lambda^2 e_{\mathrm{pw}}^H \Lambda^H \Lambda e_{\mathrm{pw}}. \tag{37}$$

This expression explicitly shows how the effective area depends on the mode efficiencies.

To relate this to gain, we first consider the transmitting case, but only the component of radiated electric field $\overline{E}$ polarized in the direction of the incident plane wave:

$$\overline{E} \cdot \hat{u}_{\mathrm{pw}} = E_{\mathrm{pw}} = \sum_n b_{2,n} \hat{e}_n \cdot \hat{u}_{\mathrm{pw}} \frac{e^{-jkr}}{r} = \sum_n b_{2,n} e_{\mathrm{pw},n} \frac{e^{-jkr}}{r}. \tag{38}$$

The realized gain pattern for this component of radiated field is

$$G_{\mathrm{pw}} = 4\pi \frac{b_2^H e_{\mathrm{pw}}^* e_{\mathrm{pw}}^T b_2}{a_1^H a_1} = 4\pi \frac{a_1^H S_{21}^H e_{\mathrm{pw}}^* e_{\mathrm{pw}}^T S_{21} a_1}{a_1^H a_1}. \tag{39}$$

As mentioned above, this gain pattern is a function of the incident waves $a_1$ and may take on a continuum of values. Because the gain has a quadratic form (Rayleigh's quotient), its maximum value occurs when the incident wave vector is the eigenvector corresponding to the largest eigenvalue [19]. However, the matrix $e_{\mathrm{pw}}^* e_{\mathrm{pw}}^T$ in (39) is an outer product of a single vector and therefore possesses only one degree of freedom. Thus, all but one of its eigenvalues are zero. It is straightforward to show that the incident wave vector $a_1 = S_{21}^H e_{\mathrm{pw}}^*(\theta_o,\phi_o)$ produces the maximum gain (in the $\theta_o,\phi_o$ direction):

$$G_{\mathrm{pw}}\Big|_{\max} = 4\pi e_{\mathrm{pw}}^T S_{21} S_{21}^H e_{\mathrm{pw}}^* = 4\pi e_{\mathrm{pw}}^H \Lambda^H \Lambda e_{\mathrm{pw}}. \tag{40}$$

To arrive at the last equality, we used reciprocity ($S_{21} = S_{12}^T$) and conjugated the (real) result. Thus, we see that the effective area

$$A_e = \frac{\lambda^2}{4\pi} G_{\mathrm{pw}}\Big|_{\max} \tag{41}$$

is proportional to the maximum realized gain pattern computed from the component of radiated electric field that lies in the direction of polarization of the incident plane wave.

In general, the mode coupling matrix $[\hat{e}^* \cdot \hat{e}^T]$ can be expressed as the product of an $N \times 2$ matrix with its conjugate transpose and therefore has only two degrees of freedom. This means that for any chosen direction, the matrix has only two nonzero eigenvalues, with the largest corresponding to maximum realized gain. This excitation produces the maximum gain with a particular polarization, and one can

show that the excitation corresponding to the other nonzero eigenvalue is the gain for the orthogonal polarization. The remaining $N-2$ zero eigenvalues correspond to the set of incident terminal port waves that produce null fields in the chosen direction.

## 5. Backscatter Modes

It is often useful to determine the incident terminal port waves that produce retrodirectively reflected waves with the same relative values, and we refer to these as backscatter modes to distinguish them from radiation modes. Mathematically, this is a conjugate eigenvalue problem where we determine the set of incident wave vectors $a_1$ that satisfy

$$S_{11}a_1 = \Gamma_n a_1^* \tag{42}$$

for a complex reflection coefficient $\Gamma_n$. If an orthonormal set of such excitations exists, collected in the columns of a matrix $V$ with the $n$th column corresponding to the eigenvalue $\Gamma_n$, it is straightforward to show that $S_{11}$ must be symmetric. Thus, we conclude that the ability to diagonalize $S_{11}$ implies terminal port reciprocity.

The unitary matrix $V$ whose columns satisfy (42) diagonalizes $S_{11}$ in the following way:

$$S_{11}V = V^*\Gamma \longrightarrow V^T S_{11} V = \Gamma, \tag{43}$$

where $\Gamma$ the diagonal matrix of eigenvalues. The matrix $V$ describes unitary transformations of the original incident and reflected terminal waves $a_1$ and $b_1$ to a new set $a_1'$ and $b_1'$ according to

$$a_1 = Va_1', \qquad b_1 = V^* b_1'. \tag{44}$$

As with the radiation modes, this transformation may be represented by a lossless, reciprocal network that has a scattering matrix

$$S_V = \begin{pmatrix} 0 & V^T \\ V & 0 \end{pmatrix}. \tag{45}$$

Inserting this network on the terminal side of the antenna (as in Figure 3 with $S_U \rightarrow S_V$) gives a net scattering matrix for the combined diagonalization network and antenna equal to

$$S' = \begin{pmatrix} V^T S_{11} V & V^T S_{12} \\ S_{21} V & S_{22} \end{pmatrix} = \begin{pmatrix} \Gamma & S_{12}' \\ S_{21}' & S_{22} \end{pmatrix}. \tag{46}$$

Thus, we see that this network diagonalizes $S_{11}$, eliminating the mutual coupling between input ports. These networks are referred to as decoupling networks and have been studied by a number of groups [11, 12, 20–22]. It is straightforward to show that for a lossless antenna the incident waves that produce the radiation and backscatter modes are identical (i.e., $U = V$).

Radiation and backscatter modes are particularly useful for providing physical insight to superdirective antennas. As the element spacing is reduced below $\lambda/2$, one finds that the radiation mode patterns overlap and the mode directivities increase in the end-fire direction (when the element factor allows it). Assuming for simplicity that the antenna elements all have identical polarization, using (32), we see that the radiated wave vector $b_2 = S_{21}a_1 = e^*$ results in the maximum possible directivity for the antenna

$$D_{\max} = 4\pi e^H e = \sum_n D_n \tag{47}$$

which is the sum of the mode directivities. The incident waves required to produce these modes is $a_1 = S_{21}^{-1} e^* = U\Lambda^{-1/2} e^*$. This result shows that higher-order, low-efficiency modes (small $\lambda_n$) require substantial incident power to produce the desired output fields. Mode efficiencies may be increased by impedance matching, and this may be greatly facilitated by a decoupling network. Since mutual coupling is eliminated, each mode input may be matched independently from the rest, achieving (in theory) simultaneous matching of all the modes. Even when decoupling network realization is impractical (as is often the case), the backscatter modal analysis is a convenient way to characterize the antenna. Each backscatter mode has a characteristic input reflection coefficient from which the modal quality factor may be computed.

## 6. Examples

*6.1. Half Wave Dipoles.* We apply the modal analysis to an ideal, perfectly conducting dipole of length $\lambda/2$, not located at the origin, but translated a distance $a$ along the $y$-axis. This will provide an analytical example using simple closed form expressions for dipole input impedance and radiated fields presented in many texts. Of course, these expressions are approximate, derived assuming a sinusoidal current distribution on the dipole and neglecting the feed discontinuity, but they are reasonably accurate and widely used in the literature. We displace the dipole from the origin to show that the theory accounts for the locations of modal phase centers which are generally not known. The dipole scattering parameters ($S_{11}$ and $S_{21}$) and mode functions will then be used to compute the mutual coupling between two dipoles (in a scattering representation) and show that our result agrees with that given by a mutual coupling formula obtained using a different method, evaluated for large dipole separation.

Assuming a sinusoidal dipole current, a $z$-oriented half wave dipole located at $y = a$ radiates a far zone electric field [23]

$$\overline{E} = j\eta_o I_1 \frac{e^{-jkr}}{2\pi r} \frac{\cos((\pi/2)\cos\theta)}{\sin\theta} e^{jka\sin\theta\cos\phi}\hat{u}_\theta \tag{48}$$

proportional to the current $I_1$ entering its terminals. This current is related to the incident wave amplitude as $\sqrt{Z_o}I_1 = (1 - S_{11})a_1$. The reflection coefficient $S_{11}$ may be computed from the input impedance of the dipole [24],

$$Z_{11} = \frac{\eta_o}{4\pi}\left(\gamma + \ln 2\pi - \mathrm{Ci}(2\pi) + j\,\mathrm{Si}(2\pi)\right), \tag{49}$$

where $\gamma$ is Euler's constant and Ci and Si are the cosine and sine integrals.

We compute the $M$ "matrix" (a single element) by substituting (48) in (3):

$$M = \frac{\eta_o}{Z_o}|1 - S_{11}|^2 \frac{1}{4\pi}\left(\gamma + \ln 2\pi - \mathrm{Ci}(2\pi)\right) = 1 - |S_{11}|^2. \tag{50}$$

The last equality was obtained using (49). This matrix is already diagonalized, so the eigenvalue equals $M$ and the eigenvector matrix can be taken as unity. The mode function is then

$$\hat{e} = \frac{e^{jka\sin\theta\cos\phi}}{\sqrt{\pi(\gamma + \ln 2\pi - \mathrm{Ci}(2\pi))}} \frac{\cos((\pi/2)\cos\theta)}{\sin\theta}\hat{u}_\theta, \tag{51}$$

normalized to satisfy (6). Note that the phase dependence introduced by the offset phase center is included in the mode function. The parameter $\lambda_1$ is determined from (8), which, using (21), gives the scattering parameter

$$S_{21} = j\sqrt{\frac{\eta_o}{Z_o}}(1 - S_{11})\sqrt{\frac{\gamma + \ln 2\pi - \mathrm{Ci}(2\pi)}{4\pi}}, \tag{52}$$

where we have rotated the radiation port reference plane back to the origin $r = 0$.

Mutual coupling between identical half wave dipoles may be computed using (29). The mode function for a second dipole located at the origin of a new (primed) coordinate system of distance $d$ along the $y$-axis of the original system is given by

$$\hat{e}^{\mathrm{II}} = \frac{e^{-jkd}}{\sqrt{\pi(\gamma + \ln 2\pi - \mathrm{Ci}(2\pi))}} \frac{\cos((\pi/2)\cos\theta')}{\sin\theta'}\hat{u}'_\theta, \tag{53}$$

where we have defined the radiation port reference plane so that it coincides with the reference plane of the first dipole. Substituting (51), (52), and (53) in (29), we obtain, after some manipulation, the terminal-to-terminal scattering parameter

$$S_{21}^{\mathrm{total}} = -j\lambda S_{21}^I S_{12}^{II}\hat{e}^I \cdot \hat{e}^{II} = j\lambda\frac{\eta_o}{Z_o}\left(\frac{1 - S_{11}}{2\pi}\right)^2 \frac{e^{-jk(d-a)}}{d}. \tag{54}$$

For comparison, the expression for mutual coupling between ideal half-wave broadside-coupled dipoles in the limit of a large separation distance $r$ is given by [25]:

$$Z_{21}^{\mathrm{total}} = j\frac{\eta_o}{\pi}\frac{e^{-jkr}}{kr}, \tag{55}$$

where we have retained the superscript to distinguish this coupling parameter from that of a single dipole. Because $Z_{21}^{\mathrm{total}} << Z_o$, the associated scattering parameter is

$$\begin{aligned} S_{21}^{\mathrm{total}} &\cong j\frac{2}{\pi}\frac{Z_o\eta_o}{(Z_{11} + Z_o)^2}\frac{e^{-jk(d-a)}}{kd} \\ &= j\lambda\frac{\eta_o}{Z_o}\left(\frac{1 - S_{11}}{2\pi}\right)^2\frac{e^{-jk(d-a)}}{d}, \end{aligned} \tag{56}$$

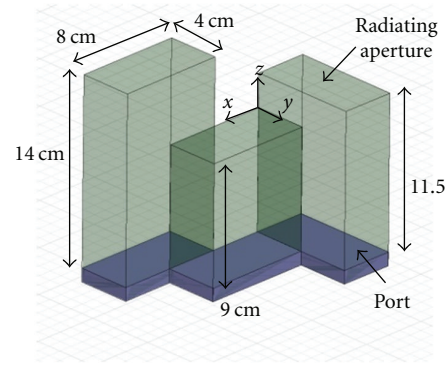


Figure 4: EM simulation model of three open-ended waveguides radiating into empty space, operating at 3 GHz. Each waveguide consists of four perfectly conducting walls, an excitation port, and a radiating aperture. The model was simulated using HFSS with perfectly matched layer (PML) boundaries in the far field.

agreeing with (54). Of course, for these simple linear antennas, the standard Z matrix approach is much simpler. But the modal method is easily generalized to arbitrary antenna elements arranged in any manner.

*6.2. Open-Ended Waveguide Array.* To show how the theory may be used in practice, we consider an array of three open ended waveguides, illustrated in Figure 4, radiating in empty space at a frequency of 3 GHz. This arrangement was chosen for its generality, including a nonplanar arrangement of radiating elements and mixed polarization. The waveguide walls are of infinitesimal thickness and their lengths finite with ideal ports located internally, as indicated in the figure.

Three sets of far zone electric fields $\overline{E}_n$ were computed using a commercial finite element simulator with 1 W of power incident from each of the three waveguide ports in succession with the unexcited ports terminated in matched loads. The matrix $M$ of overlap integrals was computed as in (3) and then diagonalized, giving the following sets of eigenvalues and eigenvectors:

$$\begin{aligned} \Lambda^H\Lambda &= \begin{pmatrix} 1.00 & 0 & 0 \\ 0 & 0.94 & 0 \\ 0 & 0 & 0.88 \end{pmatrix}, \\ U &= \begin{pmatrix} .58\angle 45^\circ & .38\angle -107^\circ & .72\angle 95^\circ \\ .77\angle 55^\circ & .13\angle -10^\circ & .63\angle -68^\circ \\ .27\angle -51^\circ & .92\angle 0.6^\circ & .29\angle 41^\circ \end{pmatrix}. \end{aligned} \tag{57}$$

Because the antennas are perfectly conducting, the matrix $U$ also diagonalizes the terminal port scattering matrix

$$S_{11} = \begin{pmatrix} .26\angle -151^\circ & .11\angle 10^\circ & .03\angle -176^\circ{}^\circ \\ .11\angle 10^\circ & .19\angle -178^\circ & .09\angle 33^\circ \\ .03\angle -176^\circ & .09\angle 33^\circ & .25\angle -10^\circ \end{pmatrix}, \tag{58}$$

in the manner of (43) ($V = U$).

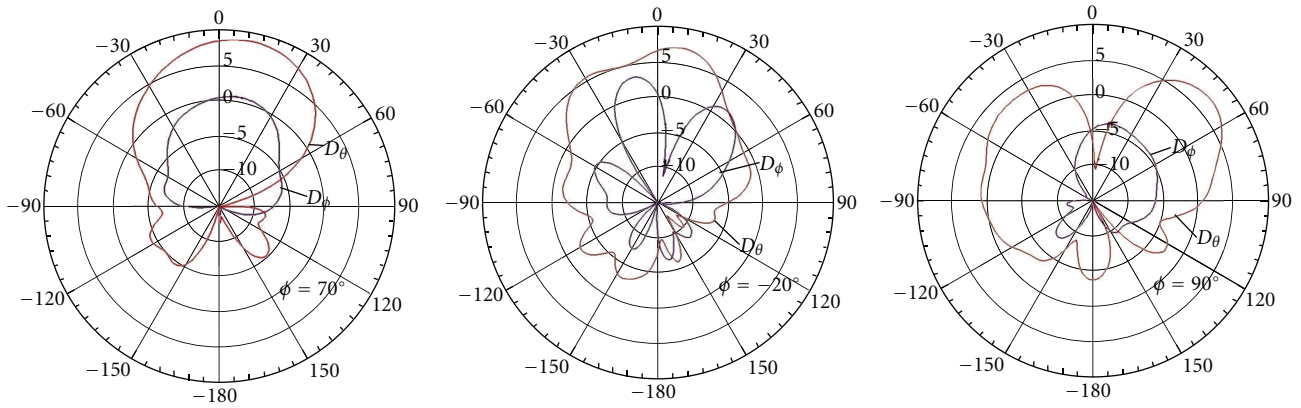


Figure 5: Plots of directivity $D$ (dB) versus theta for the three radiation modes. Each plot is taken at the phi cut containing maximum total directivity. The three modes are mutually orthogonal over the entire sphere.

Next, we use (1) to compute the modal fields $\overline{E}_n^-$ and normalize them to determine the mode functions according to

$$\hat{e}_n = \frac{\overline{E}_n^-}{\sqrt{\iint \left|\overline{E}_n^-\right|^2 d\Omega}} = \frac{r\overline{E}_n^-}{\sqrt{\eta_o}|\lambda_n|}. \tag{59}$$

Note that this particular normalization equates the phases of $\overline{E}_n^-$ and $\hat{e}_n$. A different choice would produce a corresponding phase change in the $\lambda_n$. How we allocate the phase between $\lambda_n$ and $\hat{e}_n$ in (7) is arbitrary.

Figure 5 contains plots of the modal directivity patterns in dB versus polar angle $\theta$, each taken in the plane of $\phi$ containing the maximum total directivity. The $\theta$ and $\phi$ components of directivity are plotted separately to provide more detail. The radiation scattering matrix $S_{21}$ is computed using (22):

$$S_{21} = \begin{pmatrix} .59\angle -45^\circ & .77\angle -55^\circ & .27\angle 51^\circ \\ .36\angle 107^\circ & .13\angle 10^\circ & .89\angle -0.6^\circ \\ .68\angle -95^\circ & .59\angle 68^\circ & .28\angle -41^\circ \end{pmatrix}. \tag{60}$$

Knowledge of the scattering submatrix $S_{21}$ and the mode functions $\hat{e}_n$ makes many antenna calculations straightforward. As an example, we determine the maximum possible realized gain of this antenna. We first compute the mode overlap matrix $[\hat{e}^* \cdot \hat{e}^T]_{mn} = \hat{e}_m^*(\theta,\phi) \cdot \hat{e}_n(\theta,\phi)$ and then the matrix product $C = S_{21}^H[\hat{e}^* \cdot \hat{e}^T]S_{21}$ from (34). The realized gain is maximized in the $\theta,\phi$ direction by a terminal port incident wave vector equal to the eigenvector corresponding to the largest eigenvalue of $C$, denoted $\lambda_{c,\max}(\theta,\phi)$. For the antenna considered here, the largest of all such eigenvalues occurs for $\theta = 15.5^\circ$, $\phi = 82^\circ$ (within the accuracy of our discretization of $\theta,\phi$) with a value $\lambda_{c,\max} = 0.68$. This corresponds to a maximum possible realized gain of 9.3 dB. The incident wave vector that produces this gain is

$$a_1 = \begin{pmatrix} 0.70\angle 32^\circ \\ 0.70\angle 25^\circ \\ 0.12\angle -125^\circ \end{pmatrix} \tag{61}$$

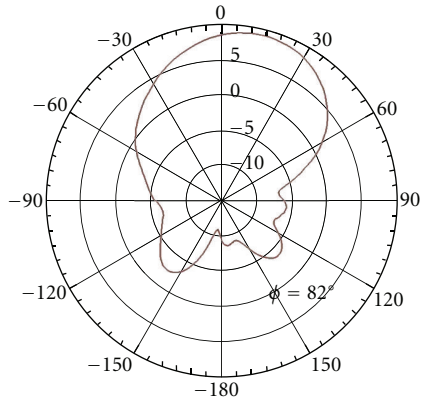


Figure 6: Plot of the realized gain (dB) versus theta for the excitation that maximizes this quantity. The phi cut is the plane containing the maximum gain value of 9.3 dB.

with a gain pattern shown in Figure 6, plotted in the $\phi$ cut containing the maximum. The unit polarization vector for this radiated field is determined using (9) with (61):

$$\hat{u}_1 = \begin{pmatrix} 1\angle 71^\circ \\ 1\angle 5^\circ \end{pmatrix}. \tag{62}$$

An excitation based on the other nonzero eigenvector of $C$ in this direction produces the orthogonal polarization

$$\hat{u}_2 = \begin{pmatrix} 1\angle -47^\circ \\ 1\angle 67^\circ \end{pmatrix} \tag{63}$$

with a corresponding gain of 6.7 dB.

## 7. Conclusion

The formalism presented in this paper provides a network description of multiport antennas, derived directly from measurements, that exactly accounts for mutual coupling

and scattering between elements. Since the radiation and reception properties of the antenna are completely described by a scattering matrix and a set of orthonormal mode functions, the approach simplifies many antenna computations and allows for easy accounting of power transfer. We believe this theory gives physical insight to superdirectivity, and will be useful for various antenna applications such as non-Foster matching of antenna arrays, direction finding, phased array beamforming, and compressive sensing.

## Appendix

## Asymptotic Evaluation of Overlap Integral

We simplify the integral (16) by rotating the coordinate system so that the plane wave is incident along the positive $z$-axis, and first asymptotically evaluate the integral over $\theta$ as $r \to \infty$:

$$I = \int_0^{\pi} f(\theta) e^{jkr\cos\theta} \sin\theta \, d\theta, \tag{A.1}$$

where $f(\theta) = \hat{u}_{pw} \cdot \hat{e}_n(\theta)$ for any $\phi$. The argument of the exponent has saddle points where its derivative vanishes, namely, $\theta = 0$ and $\theta = \pi$. Considering $\theta$ as a complex variable we integrate along a contour $C$ on the real axis from 0 to $\pi$ in the complex plane. A well-behaved function $f(\theta)$ will produce an integrand that is analytic in and around the integration contour, allowing us to deform the contour along a path for which the imaginary part of the exponent vanishes at the saddle point. Considering the saddle point at $\theta = 0$ first, the steepest decent contour satisfies

$$\mathrm{Im}(jkr\cos\theta - jkr) = 0. \tag{A.2}$$

Expressing $\theta$ in real ($\theta_r$) and imaginary ($\theta_i$) parts, we choose the contour with $\theta_r = \theta_i$ so that (A.2) is satisfied to first order near the saddle point. We then change variables so that the exponent has a quadratic exponential decay away from the saddle point using

$$w^2 = -2jkr(\cos\theta - 1) \longrightarrow w\,dw = jkr\sin\theta\,d\theta. \tag{A.3}$$

The contribution to the integral from the $\theta = 0$ saddle point is then

$$I_0 \approx \frac{e^{jkr}}{jkr} \int_0^{\infty} f(w) e^{-(1/2)w^2} w\,dw \approx f\,|_{\theta=0} \frac{e^{jkr}}{jkr}. \tag{A.4}$$

The above integral is taken over a real variable because our choice of transformation (A.3) places our integration path on the real axis in the $w$-plane. The exponential decay in the exponent allows us to integrate to infinity with little error.

The contribution from the saddle point at $\theta = \pi$ may be evaluated in a similar manner giving the complete first order asymptotic solution for (A.1) as

$$I \approx f\,|_{\theta=0} \frac{e^{jkr}}{jkr} + f\,|_{\theta=\pi} \frac{e^{-jkr}}{jkr}. \tag{A.5}$$

The evaluation of a function in spherical coordinates at $\theta = 0$ and $\theta = \pi$ eliminates the $\phi$ dependence so that the integral over $\phi$ in (16) simply gives an additional factor of $2\pi$. Rotating the coordinate system back to the original directions, we arrive at the final result

$$\iint \hat{u}_{\mathrm{pw}} \cdot \hat{e}_n(\theta_o, \phi_o) e^{jkr[\sin\theta_o \sin\theta\cos(\phi-\phi_o)+\cos\theta_o\cos\theta]} d\Omega$$
$$\approx 2\pi \left[ \hat{u}_p \cdot \hat{e}_n(\theta_o, \phi_o) \frac{e^{jkr}}{jkr} + \hat{u}_p \cdot \hat{e}_n(\pi - \theta_o, \phi_o + \pi) \frac{e^{-jkr}}{jkr} \right]. \tag{A.6}$$

The incoming and outgoing waves are both present because the "incident" plane wave exists in all space, incoming on one side of the array and outgoing on the other. It is only the incoming term that is relevant to our analysis of the receiving properties of the array.

## References


[1] E. Telatar, "Capacity of multi-antenna Gaussian channels," *European Transactions on Telecommunications*, vol. 10, no. 6, pp. 585–595, 1999.

[2] C. Waldschmidt, J. V. Hagen, and W. Wiesbeck, "Influence and modelling of mutual coupling in MIMO and diversity systems," in *Proceedings of the IEEE Antennas and Propagation Society International Symposium*, pp. 190–193, San Antonio, Tex, USA, June 2002.

[3] W. Wiesbeck and E. Heidrich, "Wide-band multiport antenna characterization by polarimetric RCS measurements," *IEEE Transactions on Antennas and Propagation*, vol. 46, no. 3, pp. 341–350, 1998.

[4] C. Waldschmidt, S. Schulteis, and W. Wiesbeck, "Complete RF system model for analysis of compact MIMO arrays," *IEEE Transactions on Vehicular Technology*, vol. 53, no. 3, pp. 579–586, 2004.

[5] A. T. De Hoop, "N-port receiving antenna and its equivalent electrical network," *Philips Research Report*, vol. 30, pp. 302–315, 1975.

[6] A. T. De Hoop, I. E. Lager, and V. Tomassetti, "The pulsed-field multiport antenna system reciprocity relation and its applications - A time-domain approach," *IEEE Transactions on Antennas and Propagation*, vol. 57, no. 3, pp. 594–605, 2009.

[7] R. F. Harrington, *Field Computation by Moment Methods*, Robert E. Krieger Publishing, Malabar, Fla, USA, 1968.

[8] R. J. Garbacz and R. H. Turpin, "Generalized expansion for radiated and scattered fields," *IEEE Transactions on Antennas and Propagation*, vol. AP-19, no. 3, pp. 348–358, 1971.

[9] R. F. Harrington and J. R. Mautz, "Theory of characteristic modes for conducting bodies," *IEEE Transactions on Antennas and Propagation*, vol. AP-19, no. 5, pp. 622–628, 1971.

[10] J. R. Mautz and R. F. Harrington, "Modal analysis of loaded n-port scatterers," *IEEE Transactions on Antennas and Propagation*, vol. AP-21, no. 2, pp. 188–199, 1973.

[11] C. Volmer, J. Weber, R. Stephan, K. Blau, and M. A. Hein, "An eigen-analysis of compact antenna arrays and its application to port decoupling," *IEEE Transactions on Antennas and Propagation*, vol. 56, no. 2, pp. 360–370, 2008.

[12] J. C. Coetzee and Y. Yu, "Port decoupling for small arrays by means of an eigenmode feed network," *IEEE Transactions on Antennas and Propagation*, vol. 56, no. 6, pp. 1587–1593, 2008.

[13] C. G. Montgomery, R. H. Dicke, and E. M. Purcell, *Principles of Microwave Engineering*, MIT Radiation Lab Series, McGraw-Hill, New York, NY, USA, 1948.

[14] J. E. Hansen, *Spherical near field antenna measurements*, Peregrinus Ltd., London, UK, 1988.
[15] A. T. De Hoop and G. De Jong, "Power reciprocity in antenna theory," *Proceedings of the Institution of Electrical Engineers*, vol. 121, no. 10, pp. 1051–1056, 1974.
[16] N. Marcuvitz, *Waveguide Handbook*, MIT Radiation Lab Series, McGraw-Hill, New York, NY, USA, 1951.
[17] R. F. Harrington, *Time Harmonic Electromagnetic Fields*, McGraw-Hill, New York, NY, USA, 2001.
[18] C. A. Balanis, *Antenna Theory: Analysis and Design*, John Wiley & Sons, New York, NY, USA, 1982.
[19] G. Strang, *Linear Algebra and Its Applications*, Academic Press, Orlando, Fla, USA, 2nd edition, 1980.
[20] W. P. Geren, C. R. Curry, and J. Andersen, "A practical technique for designing multiport coupling networks," *IEEE Transactions on Microwave Theory and Techniques*, vol. 44, no. 3, pp. 364–371, 1996.
[21] J. B. Andersen and H. H. Rasmussen, "Decoupling and descattering networks for antennas," *IEEE Transactions on Antennas and Propagation*, vol. AP-24, no. 6, pp. 841–846, 1976.
[22] H. J. Chaloupka, X. Wang, and J. C. Coetzee, "Performance enhancement of smart antennas with reduced element spacing," in *Proceedings of the IEEE Wireless Communications and Networking Conference*, vol. 1, pp. 425–430, New Orleans, La, USA, March 2003.
[23] C. A. Balanis, *Antenna Theory: Analysis and Design*, John Wiley & Sons, New York, NY, USA, 1982.
[24] Ibid., pp. 294.
[25] Ibid., pp. 299.